094013
(18)

Transport in Porous Media **36**: 85–119, 1999.
© 1999 *Kluwer Academic Publishers. Printed in the Netherlands.*

Estimates of Barometric Pumping of Moisture Through Unsaturated Fractured Rock

M. J. MARTINEZ[1] and R. H. NILSON[2]
[1]*Engineering Sciences Center, Sandia National Laboratories, Albuquerque, NM 87185, U.S.A.*
[2]*Combustion and Physical Sciences Center, Sandia National Laboratories, Albuquerque, NM 87185, U.S.A.*

(Received: 30 December 1997; in final form: 9 October 1998)

Abstract. We present a theory for the motion of water vapor at depth in a discretely fractured permeable medium induced by atmospheric barometric pressure fluctuations, or 'barometric pumping'. The theory involves multiphase mass and energy transport in a fracture/matrix system, with discrete representation of the fracture system. The barometric pressure fluctuations are approximated as periodic in time, with amplitude corresponding to measured values. To simplify the analysis, a 'single-horizon' approximation is applied in which the time-mean gradient is used to evaluate the vertical advective flux in the fractures. Time-periodic solutions are obtained numerically, enabling the calculation of the net efflux of moisture per cycle. The model is applied to material representative of the Yucca Mountain region of southwestern Nevada. The results indicate that the efflux of moisture carried upward from significant depths by barometric pumping is much less than the near surface efflux that is commonly estimated by assuming that air enters the medium dry and is returned to the atmosphere fully saturated with water vapor. This near surface efflux consists primarily of moisture discharged from the upper layer which is frequently replenished by precipitation. Of greater interest to nuclear waste repository design and estimations of net infiltration in arid regions is the fraction of the total moisture efflux that comes from significant depths. This deep transport is quantified by the fracture/matrix transport model described here. Although the transport by barometric pumping from depth is small compared to the total moisture expelled from the surface layer, it is an order of magnitude greater than the vertical moisture flux carried from depth by diffusion.

Key words: barometric pumping, two-phase flow, fractured rock.

1. Introduction

We present a theory for the motion of water vapor at depth in a fractured permeable medium induced by atmospheric barometric pressure fluctuations, or 'barometric pumping'. This mechanism may be of some importance to subsurface water vapor transport in fractured rock situated in arid regions where annual moisture infiltration is exceedingly low. This study, though motivated by the Yucca Mountain Project, is applicable to other similar sites involving fractured rock.

In such material, the fracture system is presumed to provide the primary permeability. However, the capacity of the system lies with the intact matrix. Because capillary forces will be stronger in the smaller pores of the matrix, resident liquid

14490

moisture will prefer to reside in the matrix, with the exception perhaps, of asperities or other small features of the fracture system. On the other hand, the gas, a mixture of air and water vapor, will prefer the fracture system, although it does share the void space of the matrix with liquid water. The idea behind barometric pumping, hereafter referred to as BP, is that rising barometric pressure will force ambient gas into the matrix which is drier than the resident soil gas. The latter is in thermodynamic equilibrium with resident liquid water, and is probably nearly saturated (in the thermodynamic sense) with water vapor at the prevailing temperature. The incoming dry gas will come to thermodynamic equilibrium with the soil gas, thereby humidifying the former. When the barometric pressure decreases, gas will be respired from the fractured medium, thereby discharging gas with a higher humidity than the ambient. There are two such barometric cycles of interest, the diurnal cycle and that associated with weather patterns. Typically, a weather-related barometric cycle has an average period of roughly five days (Nilson *et al.*, 1991).

1.1. A SHALLOW SUBSURFACE CONTROL VOLUME MODEL

A control volume model, which is only sensible in the shallow subsurface, can be developed to quantify the surface efflux of moisture driven mainly by barometric pressure fluctuations, but which is also influenced by several other unsteady surface processes including evapotranspiration, localized topography-induced surface pressure variations due to the 'Bernoulli' effect, and especially the episodic nature of precipitation. Collectively, these coupled processes preclude a detailed model description for the surface layer. Following the description of this control volume model, we explain why it is incapable of describing the extraction of moisture from depth due to BP. We then present the conceptual model for a theory which can relate the effects of barometric fluctuations at depth in the presence of a water vapor gradient (due to the geothermal gradient) to the upward transport of water vapor towards the shallow subsurface, where the gross extraction of moisture may be described by the control volume model. Due to the aforementioned complicating processes active at the subsurface/atmosphere interface, the net extraction of soil moisture at the surface may be different from the value calculated by the fracture/matrix theory which applies at depth. However, the fraction of the net moisture efflux due to BP from depths greater than the shallow subsurface can be quantified by the theory presented in the following.

A control volume model to estimate the amount of moisture transport by BP was derived by Tsang and Pruess (1989). They begin by using the ideal gas law to estimate the volume of gas, ΔV, that flows into or out of a porous medium during a pressure change of amplitude ΔP_g,

$$\Delta V = V_0 \frac{\Delta P_g}{P_g} = \theta_g L A \frac{\Delta P_g}{P_g}. \tag{1}$$

RECEIVED
OCT 18 2006
By

This differential volume is the product of the fractional pressure change and the subsurface air volume, V_0, with the latter written in terms of the depth to the water table, L, the volumetric gas content, θ_g, and the plan area, A, of the medium. If this gas enters the medium with a mass fraction of water vapor, $X_{v,in}$, and leaves with $X_{v,out}$, then the net outflow of water vapor is given by

$$\frac{\Delta m_v}{A} = \rho_g \theta_g L \frac{\Delta P_g}{P_g}(X_{v,out} - X_{v,in}), \tag{2}$$

where ρ_g is the mean, or nominal, gas density. By summing all such contributions from diurnal cycles of amplitude 5 mbars over a years time, Tsang and Pruess estimated, for Yucca Mountain, a net moisture discharge of 0.3 mm/year, expressed as an equivalent liquid water flux. This estimate is an upper bound because it assumes that all of the gas in the medium (of depth L) experiences the full amplitude of the barometric pressure change.

The control volume model can only account for moisture extraction occurring at or near the surface. To establish this, we first need to show that the moisture content of the gas flowing through a fracture cannot differ greatly from that of the gas residing in the adjacent permeable matrix at the same elevation. Since the fracture width, w, is no more than one or two millimeters, the transit time for diffusion of moisture from the fracture wall to the fracture center is of the order of $\Delta t = (w/2)^2/D \sim 0.1$ s for a typical gas phase diffusivity (D) of 10^{-5} m^2/s. The time for complete equilibration of water vapor concentration across the fracture should be no more than 10 times that great, or roughly one second. Now the speed of the gas in the fracture is approximately given by

$$\begin{aligned} v &= \frac{1}{(T/2)w}\left[\theta_g B L \frac{\Delta P_g}{P_g}\right] \\ &= \frac{0.04(2\,\mathrm{m})(600\,\mathrm{m})}{43200\,\mathrm{s}(0.001\,\mathrm{m})}\frac{2\,\mathrm{kPa}}{100\,\mathrm{kPa}} \\ &= 0.03\,\mathrm{m/s}. \end{aligned} \tag{3}$$

where the quantity in square brackets is the volumetric inflow/outflow that occurs by BP during each half-cycle from a slab of porous matrix having a width equal to the fracture spacing, B, and a depth, L, equal to that of the porous medium (we used the largest pressure change supported by the data analysis of Tsang and Pruess). Roughly that much gas flows through a typical fracture of width w in a half-period $T/2$, here taken as a half-day in the above estimate for a diurnal barometric cycle.

Combining the above estimates of speed and equilibration time, we conclude that the dry air entering a fracture in a partially saturated medium should travel a distance no greater than $v\Delta t = 0.03$ m, certainly no more than a meter, before the water vapor concentration in the incoming gas reaches equilibrium with that in the wall rock. Thus, the incoming gas should be fully humidified within less than a meter. Although the incoming air may then travel deeper into the formation before it

returns to the surface and is finally expelled, any significant net moisture loss from the formation will have come from the surface layer where the incoming dry air was initially humidified.

So long as the surface layer of the formation remains at least partially saturated, the gas expelled from fractures will have a relative humidity of nearly 100%, and the net rate of extraction will be consistent with the upper bound proposed by Tsang and Pruess. However, consider that in the absence of recharge, repeated cycles of BP (reinforced by surface evaporation but opposed by capillary suction) will eventually dry out the upper layer to the extent that liquid water is no longer present near the surface. The relative humidity of the air in this upper liquid-free layer would then vary from 100% at its lower surface to nearly zero at the upper surface. Under these circumstances, the simple conceptual model outlined earlier would suggest that there is no net efflux of water vapor, since $X_{v,out}$ would then be equal to $X_{v,in}$, both nearly zero. These observations illustrate that the surface moisture flux is strongly dependent on the frequency and magnitude of recharge events as well as the local balance between BP, surface evaporation, and capillary suction. The surface region is in a constantly changing state. Hence, the origin of the moisture expelled at the surface is due to many factors in addition to BP, and the amount contributed from depth by BP cannot be calculated via Equation (2). Rather than focusing on these near-surface processes, we turn our attention to greater depths, where we can propose a rational theory able to describe the contribution to the net efflux of moisture due solely to BP.

1.2. BAROMETRIC PUMPING OF MOISTURE FROM DEPTH

At every elevation between the water table and the earth's surface there is a vertical gradient in the concentration (or partial pressure) of the water vapor contained within the pores of a geologic formation. In partially saturated regions, the presence of liquid water ensures that the relative humidity will be 100% and that the local vapor pressure will be identically equal to the thermodynamic 'saturation' pressure corresponding to the local temperature, $P_{sat}(T)$. In these regions the vertical gradient in the water vapor concentration is controlled by the geothermal gradient, so that P_{sat} and X_v will both decrease toward the surface. This gradient will drive a diffusive vapor flux toward the surface.

In a medium containing vertical fractures, the oscillatory gas flow induced by barometric pumping will also carry with it a net vertical vapor flux at all elevations as a direct consequence of the vertical concentration gradient. This flux occurs because the gas in the fracture at any elevation has a slightly higher vapor content during the exhalation phase (when it is coming from a lower elevation of higher vapor concentration) than it does during inhalation (when it is coming from a higher elevation of lower concentration). The net efflux at the surface can still be expressed by the equation suggested by Tsang and Pruess, our Equation (2), but the difference in vapor content between inflow and outflow, $X_{v,out} - X_{v,in}$, is now controlled not

only by the surface processes described earlier, but also by the competition between vertical advection of moisture in the fracture and the horizontal exchange of moisture between the gas in the fracture and that in the adjacent porous matrix.

Another possible transport mechanism is cellular natural convection induced by vertical variations in temperature and water vapor content. Although such motions could marginally occur in open fractures isolated from their surroundings, they will be strongly suppressed by lateral coupling with the matrix material in which the permeability is far too small to permit such motions. Given the small aperture of fractures and small heat capacity of the flowing gas, the temperature in the fracture at a given elevation cannot be too different from the surrounding matrix temperature; this would also suppress the thermal driving potential for convection.

The net transport of heat or a chemical species by this oscillatory flow phenomenon has been previously studied by Kurzweg (1985), Nilson *et al.* (1991), and Zhao and Cheng (1996). Kurzweg originally demonstrated, both analytically and experimentally, that a very large axial heat flux can be obtained by inducing an oscillatory flow in a fluid bounded by closely-spaced heat-conducting walls. He showed that the axial heat transfer may be orders of magnitude greater than that by heat conduction, even though there is no net mass transport along the channel. Zhao and Cheng find similar behavior and provide a correlation equation for Nusselt number. Nilson later extended Kurzweg's analysis to situations in which a gas phase contaminant species is transported through a fractured permeable medium by BP; that model was more recently used by Nilson and Martinez to estimate the vertical transport of inert gas phase contaminants at Yucca Mountain (Chapter 21 of Wilson *et al.*, 1994).

The remainder of this paper investigates the transport of water vapor through a vertical gradient by this same oscillatory flow mechanism. Although this process resembles the transport of an inert gas species, the coupling between the fracture flow and the matrix transport is qualitatively altered by the occurrence of evaporation and condensation within the matrix and at the fracture/matrix interface. To describe these processes we numerically solve the equations governing mass and energy conservation for two-phase, two-component flow of air and water in the fracture/matrix system. To simplify the analysis, we use a 'single-horizon' approximation in which the time-mean gradient is used to evaluate the vertical advective flux. This approach is explained in some detail and is verified for contaminant transport by comparison with fully two-dimensional simulations.

The paper is arranged in the following way. For completeness, the general model of two-phase air/water transport in a fractured rock system is presented first. The single-horizon approximation to the model is presented next. This discussion culminates with a detailed account of the exact equations that are solved, and explains the coupling between fractures and matrix. The numerical method applied is then presented. In this part of the paper, some special attention is paid to the derivation and application of numerical boundary conditions appropriate to the two-phase, fracture/matrix system. The model is applied to materials characteristic of the Yucca Mountain region of southwestern Nevada, a site under study for possible placement

of a high-level radioactive waste repository. We find that the net vertical flow of moisture coming from significant depths via BP is no more than 3% of the upper-bound near-surface estimate suggested by Tsang and Pruess (1989). Even so, our estimates are still about one order of magnitude greater than the vertical diffusion flux (in the absence of BP) and may represent a significant fraction of the net infiltration, a quantity of great interest but even greater uncertainty.

2. Problem Formulation

In this section we present the mathematical model describing the transport of mass and energy in the fractured system. This is a necessary prelude to the discussion of the single-horizon model, which simplifies the equations to be solved, and is presented in the next section. In our mathematical description we write equations governing the transport in the fractures and matrix separately. However, the equations contain terms which describe the transfer of material and energy between the fracture and matrix systems. We neglect the flow in the matrix moving parallel to the fractures, since the associated mass flow is smaller by the ratio of matrix permeability to bulk formation permeability ($< 10^{-3}$).

The connectivity and topology of fractured formations is highly complex. Some regions of the fractures may contain deposits and fillings. Nevertheless, experimental data shows the fracture systems are connected over large depths and provide significant bulk permeability for the movement of contaminant-laden gases (Nilson *et al.*, 1991, 1992). Our representation, shown in Figure 1, is perhaps the simplest model which retains the essential features of fractured media. The bulk permeability for the two-dimensional fractured porous material model is expressed as

$$k_b = k_f \frac{w}{B} + k_m \frac{B - w}{B}, \tag{4}$$

where k_f is the fracture permeability, w is an effective fracture aperture, B is the fracture spacing, and k_m is the matrix permeability. The fracture permeability is

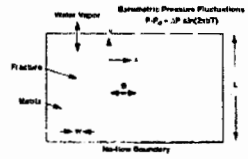

Figure 1. Conceptual model of the fractured permeable medium.

related to the effective hydraulic aperture by the formula for flow in a slot (planar Hagen–Poiseuille flow).

$$k_f = \frac{w^2}{12}. \tag{5}$$

For material properties typical of fractured rock systems (e.g. Yucca Mountain), $k_f \gg k_m$ and $w \ll B$, such that the permeability due to the fracture system dominates, resulting in the approximate expression for the bulk permeability

$$k_b = \frac{w^3}{12B}. \tag{6}$$

2.1. FRACTURE MODEL

In the fractures, we assume that only gas is present. The fractures are characterized by such large pores that capillary forces are negligible, relative to the matrix. Any liquid water condensed from the gas stream would be absorbed by the high capillary suction in the matrix before traveling any appreciable distance along the fracture. Similarly, appreciable amounts of film water are assumed not to accumulate, as they would be imbibed by the matrix. The equations are averaged over the width of the fractures and so quantities of interest vary only along the path of the fracture. In this particular application, the fractures are assumed vertical, and the coordinate y (positive upward) measures distance along the fracture. The gas flow in the fracture is governed by a mass balance equation which applies to the mixture of air and water vapor that is transported vertically up and down the fracture. The horizontal mass flux contributed from the adjoining matrix is included. The statement of this balance allows evaporation and condensation of moisture at the fracture/matrix interface to convert liquid into vapor or vice versa, as required to satisfy the imposed condition of negligible liquid in the fractures. The balance equation for the gas in the fractures is

$$\frac{\partial \rho_g}{\partial t} + \frac{\partial}{\partial y}(\rho_g q_{gy}) = -\frac{2}{w}(F_l + F_g), \tag{7}$$

where ρ_g is the density of the gaseous mixture composed of air and water vapor, q_{gy} is the (vertical) flux of gas, and F_l and F_g denote the mass fluxes of liquid and gas leaving (entering) the fracture to (from) the matrix. In the remainder of this work, subscript g refers to gas, v to water vapor, a to air, l to liquid and m to moisture (liquid and vapor). A balance equation for the water vapor in the fracture is also specified in order to compute the mass fraction of gas attributable to water vapor:

$$\rho_g \frac{\partial X_v}{\partial t} + \rho_g q_{gy} \frac{\partial X_v}{\partial y} = -\frac{2}{w}[F_l(1 - X_v) + J_v], \tag{8}$$

where

$$X_v = \frac{\rho_v}{\rho_v + \rho_a} \tag{9}$$

is the mass fraction of water vapor in the gas, and J_v denotes the horizontal diffusive flux of water vapor through air in the matrix. The overall gas balance equation (7) has been used in arriving at this form, and continuity between the mass fraction of water vapor in the fracture and matrix was imposed.

An energy balance is derived in a similar manner to account for energy transported along the fracture and between the matrix and fracture:

$$\frac{\partial}{\partial t}[\rho_g(X_a u_a + X_v u_v)] + \frac{\partial}{\partial y}[\rho_g(X_a h_a + X_v h_v) q_{gy}] = -\frac{2}{w}(q_h), \tag{10}$$

where u denotes internal energy and h enthalpy, X_a is mass fraction of air in the gas, and q_h is the net heat flux from the matrix.

In order to determine the exchange terms in the foregoing equations (the quantities in brackets on the right-hand-sides), the matrix model must be specified.

2.2. MATRIX MODEL

A balance equation for matrix water, including liquid and vapor phases is given by

$$\frac{\partial}{\partial t}(\rho_l \theta_l + \rho_v \theta_g) + \nabla \cdot \mathbf{F}_m = 0, \tag{11}$$

where θ_l is the volumetric liquid moisture content, θ_g the volumetric gas content, and $\theta_l + \theta_g = \phi$, where ϕ is the porosity. The flux of moisture is

$$\mathbf{F}_m = \rho_l \mathbf{q}_l + X_v \rho_g \mathbf{q}_g + \mathbf{J}_v. \tag{12}$$

Starting from the left, the terms on the RHS represent the mass flux of liquid, the advective mass flux of water vapor and the diffusive flux of water vapor, respectively. A balance equation for air reads

$$\frac{\partial}{\partial t}(\rho_a \theta_g) + \nabla \cdot \mathbf{F}_a = 0, \tag{13}$$

where

$$\mathbf{F}_a = X_a \rho_g \mathbf{q}_g + \mathbf{J}_a. \tag{14}$$

An energy balance takes the form

$$\frac{\partial}{\partial t}\{[(1 - \phi)\rho_s C_s + \rho_l C_l \theta_l + \rho_g C_g \theta_g](T - T_0)\} + \nabla \cdot \mathbf{q}_h = Q, \tag{15}$$

where

$$C_g = C_{va} X_a + C_{vv} X_v. \tag{16}$$

$C_{\alpha v}$ is the constant volume specific heat of component α, T_0 is a reference temperature, and Q is an extraneous heat source.

2.2.1. *Constitutive Relations*

The advective fluxes are described by the extended Darcy law, in which relative permeabilities are introduced to account for the multiphase motion of fluids. Thus, the mass flux of liquid is

$$\rho_l \mathbf{q}_l = \mathbf{F}_l = -\frac{\rho_l k_m k_{rl}}{\mu_l}(\nabla P_l + \rho_l g \nabla y), \tag{17}$$

and the mass flux of gas is

$$\rho_g \mathbf{q}_g = \mathbf{F}_g = -\frac{\rho_g k_m k_{rg}}{\mu_g}(\nabla P_g + \rho_g g \nabla y), \tag{18}$$

where P is pressure, g is the gravitational acceleration, and μ is dynamic viscosity. The diffusive flux of water vapor in air is given by

$$\mathbf{J}_v = -\rho_g D_{va} \nabla X_v, \tag{19}$$

where D_{va} is the binary diffusion coefficient (see Appendix A). In accordance with mass conservation for the binary mixture, $\mathbf{J}_a = -\mathbf{J}_v$.

The capillary pressure provides the relationship between the liquid and gas phase pressures:

$$P_c \equiv P_g - P_l = \hat{P}_c(\theta_l), \tag{20}$$

which, as indicated, is assumed to be empirically specified as a function of liquid moisture content in the matrix. It is well-known that, under thermodynamic equilibrium, the vapor-pressure across a curved interface is lower than that across a flat interface. The vapor pressure is specified according to Kelvin's equation of vapor pressure lowering (Edlefsen and Anderson, 1943):

$$P_v = P_{vs}(T) \exp\left(-\frac{P_c}{\rho_l R_v T}\right), \tag{21}$$

where P_{vs} denotes the flat-interface saturation vapor pressure.

The heat flux includes conduction and convective contributions,

$$\mathbf{q}_h = -\lambda \nabla T + h_v \mathbf{F}_v + h_a \mathbf{F}_a + h_l \mathbf{F}_l, \tag{22}$$

where λ is an effective thermal conductivity and we have introduced the shorthand notation for mass fluxes: $\mathbf{F}_v = X_v \mathbf{F}_g + \mathbf{J}_v$, and $\mathbf{F}_a = X_a \mathbf{F}_g + \mathbf{J}_a$. The enthalpies are defined by $h_\alpha = C_{p\alpha}(T - T_0)$, with α = a or l, and $h_v = \Delta h_{fg} + C_{pl}(T - T_0)$, where Δh_{fg} is the latent heat of water vapor at reference temperature T_0.

The remaining thermodynamic equations of state and constitutive relations for transport properties are discussed further in the applications section and are given in Appendix A.

2.3. FRACTURE–MATRIX COUPLING

The coupling of the fracture equations to the matrix equations is explicit in balance equations set forth in Section 2.1, each of which includes a mass or energy contribution from the matrix. The matrix equations are coupled to the fracture system via fracture/matrix interface conditions requiring continuity of pressure, temperature, and vapor pressure; the fracture equations serve as Dirichlet boundary conditions on the matrix equations. The capillary pressure in the matrix at the fracture/matrix interface is specified from the Kelvin equation (21). However, the fracture is assumed to be characterized by such large pores that capillary pressure is negligible. To close the system of equations, we require that the mass fractions of air and water vapor (hence the vapor pressure) must be continuous at the fracture/matrix interface. The Kelvin equation couples the vapor pressure, temperature and matrix capillary pressure.

3. The Single-Horizon Approximation

3.1. MOTIVATION AND APPLICATION TO CONTAMINANT TRANSPORT

Direct numerical simulation of the highly nonlinear coupled fracture/matrix transient model is a computationally intensive task. Indeed, simulations of the analog problem for contaminant transport (Nilson *et al.*, 1991; Appendix B), which is governed by a *linear* transport equation, required several days of computing time for each parameter variation. The single-horizon approximation greatly simplifies the mathematical problem and reduces the computational requirements of a full multidimensional simulation. Yet, this method has proved extremely beneficial to the understanding of similar oscillatory transport problems (Kurzweg, 1985; Nilson *et al.*, 1991). The essence of the single-horizon approximation is that the advection term in the fracture equations is evaluated using the time average of the vertical concentration gradient, while the matrix transport is estimated based on a one-dimensional analysis of horizontal transport into the matrix. In Appendix B, we further demonstrate the efficacy of the single-horizon approximation as applied to contaminant transport, an analog to the subject problem. That study compares numerical solutions of the full two-dimensional transport problem, in which both the fractures and matrix are discretized, with the single-horizon approximation. The single-horizon solutions reproduce the full simulation results over a large parameter range, and at greatly reduced computer processing time. These results and the previously mentioned studies demonstrate the effectiveness of the single-horizon approximation for these time-periodic problems, because, on average, the advective transport terms in the fractures are well-approximated by replacing the vertical gradients with the time-mean background values.

3.2. SINGLE-HORIZON APPROXIMATION FOR MOISTURE TRANSPORT

The first step in applying the single-horizon approach is to derive a depth averaged mass balance in the fracture. Integrating the balance of gas in the fracture (Equation (7)) over the depth L results in

$$\rho_g q_{gy} = -\frac{2L}{w}(F_l + F_g)_{x=0^+}. \tag{23}$$

This equation relates the flux of gas in the fracture at the inlet to the fractured system, i.e., at the elevation L, to the flux of material contributed from the matrix over the length of the fracture. This integral over the length of the fracture is represented by the product of L and the quantity in brackets. The '+' superscript denotes the interface as approached from the matrix. In this form, the matrix fluxes of liquid and gas now represent depth-averaged quantities. In addition, we have neglected the slight temporal change in gas density over the length of the fracture, $\mathrm{d}(\int \rho_g \mathrm{d}y)/\mathrm{d}t$, and its effect in modulating the flux at elevation L above the lower boundary. Note that, this statement of gas balance includes the possibility of evaporation/condensation of water at the fracture/matrix interface. A balance equation for the water vapor in the fracture in the single-horizon approximation is given by (cf. Equation (8))

$$\frac{\partial X_v}{\partial t} + q_{gy}\left\langle\frac{\partial X_v}{\partial y}\right\rangle = -\frac{2}{\rho_g w}[F_l(1 - X_v) + J_v]_{x=0^+}, \tag{24}$$

where the depth-averaged vertical gradient of water vapor ($\langle \partial X_v/\partial y\rangle$) has replaced the local gradient in the advective term. Similarly, the energy equation in the single-horizon approximation is given by

$$\begin{aligned}\rho_g C_{pg}\frac{\partial T}{\partial t} + \rho_g q_{gy}\left[C_{pg}\left\langle\frac{\partial T}{\partial y}\right\rangle + (C_{pv} - C_{pa})(T - T_0)\left\langle\frac{\partial X_v}{\partial y}\right\rangle\right] - \\ -\frac{\partial P_g}{\partial t} + \rho_g(C_{pv} - C_{pa})(T - T_0)\frac{\partial X_v}{\partial t} \\ = -\frac{2}{w}\left[-\lambda\frac{\partial T}{\partial x} - F_l(h_p - h_l) + J_v\langle h_v - h_a\rangle\right]_{x=0^+},\end{aligned} \tag{25}$$

where $h_g = X_v h_v + X_a h_a$. The vertical gradients in the fracture are approximated by the average background gradients discussed earlier.

The foregoing constitute the balance equations (Equations (23)–(25)) for the fracture system in the single-horizon approximation. The balance equations in the matrix are the one-dimensional version (i.e. replace $\nabla\cdot(\,)$ with $\partial(\,)/\partial x$, etc.) of the equations given in Section 2.2. Boundary conditions for the matrix equations are provided by the requirement of continuity of total pressure, temperature, vapor pressure at the fracture/matrix interface. Specifically, the fracture equations (Equations (23)–(25)), via continuity requirements, impose Dirichlet boundary conditions for the matrix equations at the fracture/matrix interface. No-flow conditions are imposed on the matrix equations at the mid-plane of the matrix blocks depicted in Figure 1. Section 4.1 discusses the solution procedure explicitly.

4. Numerical Treatment

The foregoing governing equations constitute a coupled set of highly nonlinear partial differential equations (PDEs). The numerical method applied for solving the coupled system of parabolic PDEs is the so-called Method-of-Lines (MOL) (Hyman, 1979). The MOL technique is a semi-discretization method wherein the spatial derivatives are first approximated by some appropriate method (in this case, centered finite differences), resulting in a system of coupled ordinary differential equations (ODEs) describing the temporal variation of the state variables at a number of discrete points. The resulting system of ODEs is integrated forward in time by the variable-order, variable-step backward-difference code DEBDF (Shampine and Watts, 1980). The backward-difference formulae result in systems of nonlinear algebraic equations to be solved for nodal quantities. These equations are solved as part of the DEBDF package via a Newton-type algorithm.

In the present application, we will assume the matrix always contains some liquid water. Hence, we choose as primary variables the capillary pressure, the gas pressure and temperature. Approximating the spatial divergences in Equations (11), (13) and (15) by centered differences, the system of discrete ODEs describing the temporal variation of primary variables at node points takes the form

$$\begin{bmatrix} C_{\psi} & 0 & C_{\psi T} \\ C_{p\psi} & C_P & C_{PT} \\ C_{T\psi} & C_{TP} & C_T \end{bmatrix}_i \begin{bmatrix} \dot{P}_c \\ \dot{P}_g \\ \dot{T} \end{bmatrix}_i = \frac{1}{x_{i+1/2} - x_{i-1/2}} \begin{bmatrix} F_{m,i+1/2} - F_{m,i-1/2} \\ F_{a,i+1/2} - F_{a,i-1/2} \\ q_{h,i+1/2} - q_{h,i-1/2} \end{bmatrix} + \begin{bmatrix} 0 \\ 0 \\ Q \end{bmatrix}_i \tag{26}$$

for a mesh of nodes with node points at x_i. Each flux is also expressed as a centered difference (on a staggered mesh), for example,

$$F_{l,i+1/2} = -\left(\frac{\rho_l k_m k_{rl}}{\mu_l}\right)_{i+1/2} \frac{P_{l,i+1} - P_{l,i}}{x_{i+1} - x_i}. \tag{27}$$

The capacitance matrix is given by

$$\begin{bmatrix} C_{\psi} & 0 & C_{\psi T} \\ C_{p\psi} & C_P & C_{PT} \\ C_{T\psi} & C_{TP} & C_T \end{bmatrix}^{\mathrm{T}} = \begin{bmatrix} \dfrac{\partial}{\partial P_c} \\ \dfrac{\partial}{\partial P_g} \\ \dfrac{\partial}{\partial T} \end{bmatrix} [(\rho_l\theta_l + \rho_v\theta_g)\ (\rho_v\theta_g)\ u], \tag{28}$$

where u denotes the bulk internal energy. After evaluating the fluxes and capacitance matrix, the 3×3 system of Equations (26) that apply at each grid point are inverted to obtain the time derivatives needed by the ODE solver.

Verification of this two-component, two-phase code is discussed in Martinez (1995).

4.1. BOUNDARY COUPLING FUNCTIONS

The Equations (23)–(25) describe the transport of gas, water vapor and energy in the fracture for the single-horizon model and constitute the boundary conditions applied to the matrix equations, as explained next. The objective is to solve the discrete matrix equations (Equation (26)) in order to determine the net efflux of moisture at a representative horizon. Specifically, the fracture equations in the single-horizon approximation are used to prescribe boundary conditions on the equations for P_g, P_c, and $\dot{T}$ (the over-dot denotes a time derivative) which appear in the discrete matrix equations, Equation (26). The barometric pressure is modeled with a sinusoid, $P_g(t) = P_0 + \Delta P \sin(2\pi t/T)$, and therefore $\dot{P}_g$ is also a circular function. $\dot{T}$ is given by Equation (25). This expression involves $\dot{P}_g$, $\dot{X}_v$, which is determined by differentiation of Equation (9), and the convective and diffusive fluxes of heat from the matrix, the quantities in brackets on the right-hand-side of Equation (25).

The boundary condition for P_c to be applied to Equation (26) is derived by enforcing the continuity of vapor pressure at the fracture/matrix interface. This is accomplished by first deriving an expression for the time derivative (denoted by over-dot) of the vapor pressure, which can be related to time derivatives of the state variables according to

$$\dot{P}_v = \frac{[(X_v \dot{P}_g + \dot{X}_v P_g - \dot{X}_v P_c) M_a/M_v + \dot{X}_v P_c]}{1 + X_v(M_a/M_v)}. \tag{29}$$

This equation is derived from the definition of the vapor mass fraction, Equation (9), and the equations of state given in Appendix A. Now, using the Kelvin equation, the time rate of change of the capillary pressure is given by

$$\dot{P}_c = \frac{\rho_l}{\rho_v}\dot{P}_v + \left[\frac{\rho_l R_v T}{P_{vs}}\left(\frac{\mathrm{d}P_{vs}}{\mathrm{d}T}\right) + \frac{P_c}{T}\right]\dot{T}, \tag{30}$$

in which $\dot{P}_v$ is given by the preceding expression, thereby completing the specification of coupling functions at the fracture/matrix interface.

To summarize, the numerical solution in the single-horizon approximation involves solving the three discrete matrix equations given in Equation (26) subject to the fracture/matrix interface conditions, which serve as boundary conditions. At the fracture/matrix interface, P_c is given by Equation (30), $\dot{T}$ is given by Equation (25) (after substituting for $\dot{P}_v$ from Equation (29)), and $\dot{P}_g$ is given by differentiating the sinusoid specifying the gas pressure in the fracture. For the BP simulations the 'unit cell' includes only half the matrix block. No-flow boundary conditions are imposed for moisture, air and energy at the center of these blocks. Once a time-periodic solution is obtained, Equation (23) is used to compute the net efflux of moisture from depth.

5. Barometric Pumping of Water Vapor

5.1. THE BACKGROUND GRADIENT

In order to establish a 'nominal' state of the fractured medium in the presence of the geothermal gradient, we reconsider a problem discussed by Tsang and Pruess (1989, 1990) in a study of gas flow at Yucca Mountain. We consider one-dimensional two-phase flow of air and water along a 600 m depth of unfractured medium over which a temperature gradient is imposed. This corresponds to the depth to the water table at Yucca Mountain, and material properties representative of the Topopah Springs unit, which is being considered for placement of a high-level nuclear waste repository, are specified over the entire depth. The lower boundary is assumed saturated with liquid water, and at a temperature of 30.85°C and pressure of 1 bar. The upper boundary, which represents the top of Yucca Mountain and therefore the interface with the ambient, is at 12.85°C and 0.9334 bar, see Tsang and Pruess (1989). We note that, this is a gross over-simplification of the geology of Yucca Mountain, however the intent is to compute a mountain-scale water vapor background gradient on which to superimpose the barometric pressure fluctuation.

Beginning with arbitrary initial conditions, we march the ODEs forward in time until a steady state is achieved. The liquid saturation and mass flux profiles computed in this manner agree well with those given by Tsang and Pruess (1989, 1990). The simulation establishes an average vapor mass fraction gradient, $(\mathrm{d}X_v/\mathrm{d}y) = -3.24\times10^{-5}\ \mathrm{m}^{-1}$ owing to the imposed background geothermal gradient $(\mathrm{d}T/\mathrm{d}y) = -0.03°\mathrm{C/m}$. These values will be used for the background gradients upon which will be superposed a periodic variation in pressure. As an aside, it is of interest to note that the net flux of water vapor implied by these gradients is of the order of 0.5×10^{-4} mm/yr. This is the flux implied by the geothermal gradient in an unfractured rock mass composed entirely of intact matrix rock; it is quite a bit smaller than the theoretical upper bound described by the control volume model and also smaller than the contribution from depth due to BP, to be presented shortly.

5.2. FIGURES OF MERIT

In order to quantify the transport of water vapor by BP, we define here several quantities characterizing the motion. The distance traveled by the gas in a half-period of outflow (hence, the absolute value), is defined by

$$\Delta L = \int_t^{t+T} \max(q_{gy}, 0)\,\mathrm{d}t, \tag{31}$$

where T denotes the time period of the barometric pressure fluctuation. The respired mass flux of moisture per fracture per barometric cycle is computed according to,

$$\Delta M_v = \int_t^{t+T} \rho_v q_{gy}\,\mathrm{d}t. \tag{32}$$

The amount of moisture mass removed during a cycle is $\Delta M_v w$ per fracture, and the annual net moisture respired per unit surface area by the periodic BP is

$$q_0 = \Delta M_v N_T \frac{w}{B}, \tag{33}$$

where N_T is the number of cycles per year.

5.3. GENERAL FEATURES OF THE MOTION

It is instructive to consider the general features of the motion induced by the periodic variation in barometric pressure. We discuss the solution of a 'base case' for which the equations of state and transport models are described in Appendix A, and the corresponding parameters are specified in Table I. Included in this table are the parameters which enter into the characteristic matrix material functions which are representatives of the Topopah Springs unit of Yucca Mountain (Wilson *et al.*, 1994). The values of aperture and fracture spacing in Table I correspond to a bulk permeability of $k_b = 10$ D.

The magnitude of the barometric pressure fluctuations, ΔP in Table I, was determined by Tsang and Pruess (1989) by analysis of the data collected at Yucca Mountain by Church *et al.* (1985, 1986). The initial state of the system is taken from

Table I. Standard problem parameters, $k_b = 10$ D.

Parameter	Symbol	Value
Formation depth	L	600 m
Fracture aperture	w	621 μm
Fracture spacing	B	2 m
Matrix permeability	k_m	10 μD
Tortuosity	τ	2
Barometric time period	T	5 days
Pressure amplitude	ΔP	1 kPa
Temperature gradient	(dT/dy)	-0.03°C/m
Mass fraction gradient	(dX_v/dy)	-3.24×10^{-3} m^{-1}
Binary diffusion coefficient	D^0_{va}	2.14×10^{-5} m^2/s
Binary diffusion parameter (App. A)	υ	2.334
Rock density	ρ_s	2580 kg/m^3
Rock heat capacity	C_s	840 J/kg°C
Effective conductivity (dry)	λ_D	1.74 W/m°C
Effective conductivity (wet)	λ_S	2.34 W/m°C
Porosity	ϕ	0.11
Residual moisture content	θ_R	0.0088
van-Genuchten parameter	α_v	0.0057 m^{-1}
van-Genuchten parameter	β_v	1.798

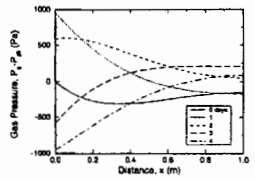

Figure 2. Profiles of gas pressure in the matrix during a 5-day barometric cycle.

the steady solution for the background gradients (discussed above) at the mid-height of the 600 m model. Specifically, the initial gas pressure is, $P_g = 0.955 \times 10^5$ Pa, the initial temperature is, $T_0 = 22.2$°C, and the initial moisture content is $\theta_i = 0.066$ (60% liquid-saturated).

Figure 2 shows the profiles of gas pressure, relative to the initial (and average) value, in the matrix at 1-day intervals during the 5-day cycle. The gas pressure in the fracture, which drives the motion, varies over ± 1 kPa and the damped pressure wave extends fully into the centerline of the matrix block for the chosen values of B and k_m. By contrast, the corresponding capillary pressure wave (not shown) extends to about 25 cm into the block and its variation is only about ± 0.02 kPa at the fracture/matrix interface. The temperature in the matrix undergoes very minute fluctuations and is not shown. The BP process for this magnitude of barometric pressure fluctuations is essentially isothermal.

Profiles of the vapor mass fraction are shown in Figure 3. They resemble a 'mirror image' of the gas pressure profiles, that is, high gas pressure at the fracture

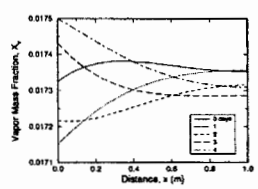

Figure 3. Profiles of vapor mass fraction in the matrix during a 5-day barometric cycle.

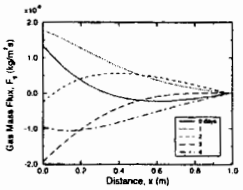

Figure 4. Profiles of gas mass flux in the matrix during a 5-day barometric cycle.

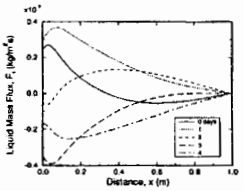

Figure 5. Profiles of liquid mass flux in the matrix during a 5-day barometric cycle.

corresponds to low vapor mass fraction at the same location, etc. The vapor mass fraction can be expressed as

$$X_v = \frac{P_v M_v}{P_v M_v + (P_g - P_v) M_a}, \tag{34}$$

therefore, increasing the gas pressure at the fracture decreases the mass fraction of water vapor for (nearly) constant vapor pressure. This sets up a diffusive flux of water vapor towards the fracture, to equilibrate the water vapor gradient.

Profiles of the mass flux of gas and liquid are shown in Figures 4 and 5. The average mass flux of the gaseous mixture is driven only by the gas pressure gradient, and the flux profiles are readily understood by comparing with Figure 2. Note that either mass flux can be in both directions at the same time owing to the time lag of points deeper into the block with respect to locations closer to the fracture wall. Beyond about 20 cm into the block, the liquid flux profiles resemble the gas flux profiles. In this region, the capillary pressure gradient is negligible and the liquid

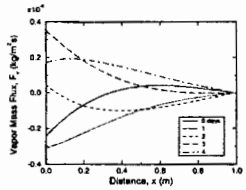

Figure 6. Profiles of vapor mass flux in the matrix during a 5-day barometric cycle.

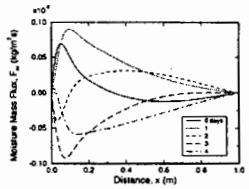

Figure 7. Profiles of moisture (liquid and vapor) mass flux in the matrix during a 5-day barometric cycle.

and gas pressure gradients are similar. The mass flux of liquid is about an order-of-magnitude less than the gas flux. The flux of water vapor is shown in Figure 6. Note that the flux is in a direction *opposite* to the average gas flux, for the reasons discussed earlier. This mechanism enables transport of water vapor from the matrix to the fracture (and vice versa) in the presence of an opposing gas pressure gradient.

The net mass flux of moisture (including liquid water and water vapor) is shown in Figure 7. The fracture model balances the mass flux of material flowing out of the matrix with the transport up and down the fracture, thereby acting as a throttle to control the amount of moisture which can be extracted from the matrix and carried by the fracture. Although the matrix liquid and vapor fluxes are of comparable magnitude to the air flux at the fracture, they sum to yield a much smaller net flux of moisture into or out of the fracture. Apparently, the net extraction of matrix moisture is determined by the amount the fracture can transport with the prevailing gas flux and thermodynamic conditions consistent with the adjoining matrix conditions.

For the base case problem just described, the gas displacement over a cycle was determined to be $\Delta L = 556.5$ m, while the net efflux of water vapor evaluated from Equation (32) was $\Delta M_v = 0.130\,\mathrm{kg/m^2}$ per cycle. Thus, according to Equation (33), the net moisture respired is $q_0 = 0.0029$ mm/yr, expressed as an equivalent annual liquid flux of water. This flux can be compared to the estimates of net infiltration discussed in Chapter 8 of Wilson *et al.* (1994), which ranges from 0.003 to 0.5 mm/yr. Thus, for the lower estimates, a significant fraction of the estimated infiltration could be extracted from deep in the formation and returned to the ambient by BP, for the present parameter values. Furthermore, this estimate for barometric transport represents only about 1% of the theoretical maximum estimated earlier by the control volume model, 0.3 mm/yr.

5.4. INFLUENCE OF MATRIX PERMEABILITY

Matrix permeability data available for Yucca Mountain (Wilson *et al.*, 1994) suggests values in the range of a few microdarcies for the welded units. In order to illustrate the role of matrix permeability, an uncertain quantity in geologic media, we consider matrix permeabilities in the range of micro- to millidarcies.

Figure 8 shows the displacement of gas in the fracture and the net efflux of moisture as a function of matrix permeability, with all other parameters as specified for the standard case. The displacement initially increases with matrix permeability, however, an asymptote is eventually attained, roughly for k_m greater than about 0.5 mD. As the permeability increases, the pressure wave is able to more easily penetrate the full extent of the matrix, ultimately resulting in equilibration between fractures and matrix for very permeable matrix material. The moisture transport exhibits a maximum for a matrix permeability of about 50 μD (for present parameters). Just as in the related problems of oscillatory heat and mass transfer, this value corresponds to a Womersly number (see Appendix B) of unity which optimizes the time scale for matrix moisture transport relative to the time period for advective fracture

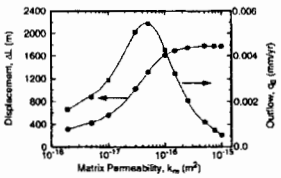

Figure 8. Gas displacement and net annual outflow as function of matrix permeability. Symbols indicate numerical values.

transport. Note that, this maximum will depend on the other problem parameters as well.

5.5. INFLUENCE OF APERTURE AND FRACTURE SPACING

The bulk permeability depends on the ratio of aperture cubed over the fracture spacing. While variation of w, for fixed B, changes the displacement, ΔL, and the amount of moisture extracted per fracture, per cycle, (ΔM_v), the net outflow of moisture is independent of w. The aperture mainly influences the gas displacement because the single-horizon model assumes that the gas flow in the fracture is unaffected by w, as appropriate when w is large enough that the vertical resistance to gas flow becomes unimportant. In this regard, our results should be viewed as an upper bound on the vertical transport.

The net respiration of moisture is dependent on B. Figure 9 shows the displacement of gas and the bulk transport of water as a function of fracture spacing. The apertures for these results were varied according to $w \sim B^{1/3}$ in order to maintain the bulk permeability constant at 10 Darcies as the fracture spacing was increased. The figure shows that both the displacement and outflow are maximized for a fracture spacing near 1 m. As the block thickness becomes large, the amount of water vapor that is extracted per fracture approaches an asymptotic value, $\Delta M_v w \rightarrow$ constant; for spacings greater than about 3 m the blocks act as though they were semi-infinite in extent (perpendicular to the fractures), and the water vapor extracted per fracture becomes independent of B. Therefore, in this regime $q_0 B \rightarrow$ const., as indicated in Figure 9. The displacement, the respiration flux per fracture, and the net efflux of water vapor also decrease as the spacing becomes small. The smaller the spacing, the more accessible is the resident moisture to be extracted, resulting in equilibration between fracture and matrix. As in the aforementioned problems of oscillatory heat and mass transfer, these conditions reduce the time-phase difference

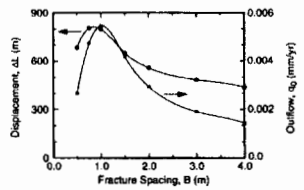

Figure 9. Gas displacement and annual net outflow as a function of fracture spacing for constant bulk permeability (10 D).

between fracture and matrix, and lead to a minimal net transport over the cycle (see Appendix B).

5.6. THE DIURNAL AND COMBINED BAROMETRIC CYCLES

In the foregoing analysis, we have only considered the 5-day barometric cycle. The simulations indicate that this cycle is more effective in extracting moisture than the diurnal cycle, for which measured variations in barometric pressure are about 8 millibars peak-to-peak. This is less than half the 20 millibars (peak-to-peak) used for the 5-day cycle, and the numerical simulations show the respiration varies quadratically with the pressure amplitude, other parameters remaining fixed. Indeed, we simulated the base case for the diurnal cycle and computed a net outflow, $q_0 = 0.001$ mm/yr, which is about one-third the outflow for the 5-day cycle (the reduction is not simply $(8/20)^2$ because we've also shortened the period of the fluctuation by one-fifth). The displacement for the one-day cycle was $\Delta L = 98.24$ m.

Thus, we have considered separately the two major barometric cycles (a 5-day weather-related cycle and the diurnal cycle) which drive the BP process. In reality, these two effects are not separate, but are active simultaneously. To approximate their joint effect, we will simply superpose the two cycles, resulting in

$$P_g = P_{g0} + \Delta P_{1dy} \sin\left(2\pi \frac{t}{T_{1dy}}\right) + \Delta P_{5dy} \sin\left(2\pi \frac{t}{T_{5dy}}\right), \tag{35}$$

where the subscripts 1dy and 5dy refer to the diurnal and 5-day cycles. The effect of this superposition (without time-phase lag) is to enhance the peak barometric fluctuations by about 40%.

For the base case set of parameters, but using the superposed barometric fluctuation, the displacement is 677.4 m and the outflow 0.004 mm/yr. These represent 20% and 33% increase in displacement and outflow, respectively, when compared to the 5-day cycle. Figure 10 shows the displacement and outflow as a function of matrix permeability. The trends are similar to the results in Figure 8 for the 5-day cycle.

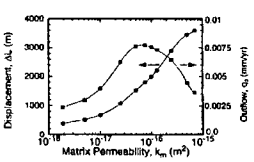

Figure 10. Gas displacement and annual net outflow as a function of matrix permeability for the combined barometric cycles.

A maximum in outflow of about 0.008 mm/yr is found for 75 μD, roughly a 40% increase over the outflow from the 5-day cycle.

6. Conclusions

We have presented a theory for the motion of air and water at depth in an unsaturated fractured permeable medium driven by fluctuations in barometric pressure. The model is of the multiple-continuum type where separate equations represent the fracture and matrix. The separate continua are coupled by transfer terms involving exchange of mass and energy between the fractures and matrix. The barometric fluctuations are approximated by a sine wave in time, with an amplitude corresponding to measured barometric fluctuations at Yucca Mountain, and with periods of one and five days. Although the model includes an energy balance, results indicate the model could be simplified by assuming isothermal conditions at the outset. To simplify the analysis, a 'single-horizon' approximation is applied in which the time-mean gradient is used to evaluate the vertical advective flux. Time-periodic numerical solutions to the governing equations are computed to estimate the moisture extraction per cycle.

Estimates of the annual net outflow of moisture from depth by BP range between 0.001 and 0.008 mm/yr, expressed as an equivalent liquid flux. This represents at most about 3% of the theoretical maximum, of 0.3 mm/yr, given by the control volume shallow subsurface model discussed in the introduction. This also represents a significant fraction of some estimates of net infiltration into Yucca Mountain (0.003–0.5 mm/yr, Wilson *et al.*, 1994), that is, a large percentage of the estimated infiltration could be respired back into the atmosphere by BP. Our estimates should be viewed as upper bounds in view of the assumptions made in applying the single-horizon approximation. Yucca Mountain is composed of alternating layers of fractured tuff and partly to nonwelded and bedded tuffs, such that the bulk permeability may vary substantially with depth, whereas our model assumes a uniform bulk permeability.

Owing to the uncertainty in material properties for geologic media in general and Yucca Mountain in particular, parameter variations of matrix permeability and fracture spacing were conducted. Maxima in the estimated outflow of moisture were found for variations of each of these parameters. The maxima are related to the time-phase lag between matrix fluxes and the barometric fluctuations driving the motion.

Appendix A. Equations of State and Transport Models

Ideal gas equations of state and mixing rules are used to approximate the thermodynamics of the system

$$\begin{aligned} P_v &= \rho_v R_v T, \qquad & P_a &= \rho_a R_a T, \\ \rho_g &= \rho_v + \rho_a, \qquad & P_g &= P_v + P_a. \end{aligned} \tag{36}$$

with $R_\alpha = \Re/M_\alpha$, for α = v or a, $\Re$ is the gas constant and M_α denotes the molecular weight. Over the range of temperatures considered in the BP problem, a function in the form of a Clapyron equation describes the flat-interface vapor pressure as a function of temperature:

$$\rho_{vs} = \rho_{v,ref} \exp\left[\frac{\Delta h_{fg}}{R_v}(T_{ref}^{-1} - T^{-1})\right] = Ae^{-B/T}. \tag{37}$$

with $A = 7.055 \times 10^5\,\mathrm{kg/m^3}$, $B = 5137.46\,\mathrm{K}$, and $P_{vs} = \rho_{vs} R_v T$.

The binary diffusion coefficient between water vapor and air is (Pruess, 1987),

$$D_{va} = \frac{\theta_g}{\tau} D_{va}^0 \frac{P_{ref}}{P_g}\left(\frac{T}{T_{ref}}\right)^{\kappa}. \tag{38}$$

where τ is tortuosity and D_{va}^0 is the diffusivity in free space at temperature T_{ref} and pressure P_{ref}. The saturation-dependent effective heat conductivity was specified according to Somerton *et al.* (1974):

$$\lambda = \lambda_0 + \frac{\theta_l}{\phi}(\lambda_1 - \lambda_0). \tag{39}$$

Moisture retention and relative permeability to the liquid are described by the so-called van Genuchten functions (van Genuchten, 1978):

$$\frac{\theta_l - \theta_{lr}}{\phi - \theta_{lr}} = (1 + p_c^{\beta_v})^{-\lambda_v}, \quad k_{rl} = (1 + p_c^{\beta_v})^{-\lambda_v/2}\left[1 - \left(\frac{p_c^{\beta_v}}{1 + p_c^{\beta_v}}\right)^{\lambda_v}\right]^2. \tag{40}$$

where $p_c = \alpha_v P_c/\rho_l g$ and $\lambda_v = (\beta_v - 1)/\beta_v$. The relative permeability to the gas is approximated by the relation (Bixler, 1985; Pruess, 1987), $k_{rl} + k_{rg} = 1$.

Appendix B. Single-Horizon Analysis of Barometric Pumping of Contaminant Gases Through Fractured Permeable Medium

The primary purpose of this appendix is to demonstrate the use of an approximate technique for analysis of quasi-steady transport induced by oscillatory gas flow in a fractured permeable medium. In particular, we will address vertical transport of an inert gas species resulting from barometric pressure variations at the earth's surface. The associated gas displacements can carry contaminated gases through hundreds of meters of fractured rock in a few months time (Nilson *et al.*, 1991, 1992). Such rapid transport has been experimentally observed at the Nevada Test Site (NTS) in volcanic rock formations which are similar to those at Yucca Mountain (YM), suggesting that the same processes will be operative at the proposed YM nuclear waste repository.

We first present numerical predictions of barometrically driven transport of an inert species at YM where the bulk permeability is believed to be an order of magnitude smaller than that at the NTS. Then, since direct numerical simulations like

these may require days of computer time, it will be shown that quasi-steady transport rates can be obtained using a single-horizon analyses which reduce computer times to minutes or seconds. The present discussion will be very brief, as further details are available in a YM publication (Nilson and Martinez, in Chapter 21 of Wilson *et al.*, 1994).

All phases of our analysis are based on a dual-porosity, dual-permeability model (Figure 1) in which identical, equally spaced fractures are separated by slabs of matrix material having uniform permeability and porosity. Flow and transport occur one-dimensionally along the fractures and one-dimensionally in and out of the matrix material. We neglect the flow moving through the matrix parallel to the fractures, since the associated mass flow is smaller by the ratio of matrix permeability to bulk formation permeability ($< 10^{-5}$).

B.1. TRANSIENT SIMULATIONS

Direct simulation of the barometric transport process requires time marching integration of the two-dimensional equations describing variations in pressure and contaminant concentration along a representative fracture and within the adjacent matrix material. The finite difference procedure described by Nilson and Lie (1990) is used to solve those equations on a rectangular mesh having 120 zones along the fracture and 40 zones into the matrix. Typically 150–300 time-steps are needed to resolve each daily barometric cycle, such that 1–10 million time-steps are executed in a simulation covering 10–100 years. These runs require 5–50 h on a Silicon Graphics R8000 computer operating at 75 MHz.

The purpose of these transient simulations is to predict the rate of release to the atmosphere of a representative puff of contaminant which initially resides at mass fraction X_0 within the porosity of a 20 m thick repository layer located 400 m below the crest of YM. For the sake of simplicity and conservatism we will ignore the 30-m layer of low permeability nonwelded tuff near the crest of YM and presume that the 600 m depth of unsaturated rock containing the repository consists of a heavily fractured welded tuff having a bulk fracture permeability ($k_b = w^3/12B$) of the order of $10^{-11}\,\mathrm{m^2}$ (10 D) which we account for through a single set of identical vertical fractures having aperture, w, and spacing, B, of 0.783 mm and 4 m, respectively. The gas filled porosity ϕ_m and gas permeability k_m of the matrix material are taken as 0.04 and 0.1 mD, while the binary diffusion coefficient D_0 and diffusion strength $\beta = \phi_m/\tau$ are prescribed as $2 \times 10^{-5}\,\mathrm{m^2/s}$ and 0.004. The transport calculation is driven by barometric pressure variations having a period and peak-to-peak amplitude of 24 h and 8 millibars, respectively.

After 40 years of pumping, the vertical variation of the normalized contaminant concentration, $X^* = X/X_0$, shown in Figure 11 has acquired a Gaussian shape spreading 200 m above and 150 m below the repository. Within 80 years, the peak concentration has fallen to roughly 10% of the initial value, while the mean holds almost steady at 3%. The profiles in Figure 11 represent concentra-

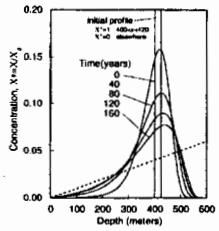

Figure 11. Concentration profiles for typical Yucca Mountain parameters.

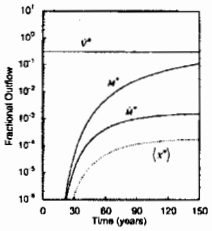

Figure 12. Normalized outflows for typical Yucca Mountain parameters.

tions at slab centers; they vary slowly in time despite daily perturbations in fracture concentrations.

The time history of gas exchange and contaminant release to the atmosphere is presented in Figure 12. The uppermost solid line, labeled $\dot{V}^*$, indicates the rate of exchange of gas between the porous formation and the atmosphere. It is calculated by integrating the outflow velocity $q_{gy} \geq 0$ from a typical fracture over the most recent barometric cycle of period T, thereafter normalizing by the total gas volume

within the corresponding unit cell ($V_0 = L(w + \phi_m B)$) and, finally, multiplying by the number N of barometric cycles occurring in a year's time:

$$\dot{V}^* = \text{fractional outflow of gas per year} = \frac{Nw}{V_0}\int_{t-T}^{t} \max(q_{gy}, 0)\,\mathrm{d}t. \qquad (41)$$

The calculated value of $\dot{V}^* = 0.3$ in Figure 12 indicates that the volume of gas which breathes out to the atmosphere and back into the medium over a year's time is 30% of the pore volume.

The rate of contaminant release to the atmosphere is also presented in Figure 12. It is calculated by integration of the instantaneous advective outflow at the earth's surface, $X\rho_g q_{gy}$, over the most recent barometric cycle

$$\dot{M}^* = \text{fractional outflow of contaminant per year} = \frac{Nw}{M_0}\int_{t-T}^{T} X\rho_g q_{gy}\,\mathrm{d}t. \qquad (42)$$

In analogy with the earlier normalization of volumetric outflow, N is the number of cycles per year and $M_0 = X_0\rho_{g0}\delta L_r(w + \phi_m B)$ is the amount of contaminant initially present in the repository layer having thickness $\delta L_r \approx 20$ m and initial mass fraction X_0. Unlike the bulk flow of gas which produces no net flux over a full cycle, there is a net flux of contaminant into the atmosphere. During periods of rising barometer, $q_{gy} < 0$ and $X^* = 0$ since the incoming gas contains only a negligible amount of contaminant. During a falling barometer, $q_{gy} > 0$ and $X^* > 0$ since the gas at the surface is coming up from below where the concentration is nonzero. Thus, the integral increases monotonically. It is seen in Figure 12 that contaminant outflow approaches a constant rate of $\sim 10^{-3}$, indicating that 0.1% of the initial contaminant inventory is being released each year.

Within 100 years, the amount of contaminant released is $\sim 10\%$, as indicated by the integrated outflow M^* shown in Figure 12. Although the numerical simulation ends at 150 years, it is possible to extrapolate into the future based on the expectation that the process will remain quasi-steady. The yearly contaminant outflow should then remain a nearly constant fraction, $\dot{M}^*$, of the current contaminant inventory, $(1 - M^*)$. Accordingly, $\mathrm{d}(1 - M^*)/\mathrm{d}t = -(1 - M^*)\dot{M}^*$ which implies that the inventory decreases exponentially as $\exp(-\dot{M}^* t)$ and that

$$M^* = 1 - \exp(-\dot{M}^* t). \qquad (43)$$

In writing this last equation we have taken the liberty of applying this quasi-steady solution for the entire time period, rather than beginning the integration at the time ($\sim$150 years) when steady state is achieved and about 10% of the contaminant has already left the medium. This adjustment is easy to make or, alternatively, the exponential solution may be viewed as a late-time complement to the early-time numerical solution. This exponential approximation avoids the need for running computations several times longer than the 40 h runs presented here.

Finally, the dotted line shown in Figure 12 indicates the average concentration of contaminant in the effluent stream

$$\langle X^* \rangle = (\dot{M}^* / \dot{V}^*)(M_0 / \rho_{g0} V_0). \tag{44}$$

It is seen to approach a nearly constant value of $\sim 10^{-4}$ which is 300 times smaller than the average subsurface concentration of $\sim 3\%$. This is to be expected because the contaminant concentration of the gases rising slowly through fractures cannot differ greatly from the local concentration in the adjacent rock. Furthermore, the time-mean concentration in the wall rock must approach zero near the surface, as seen earlier in the profiles of Figure 12. Thus, it is only the slight disequilibrium between the instantaneous fracture concentration and the time-mean wall concentration which permits a net outflow of contaminant. That is why any prediction of barometric transport requires a double porosity model which properly accounts for the disparity between fracture and wall concentrations.

B.2. QUASI-STEADY CALCULATIONS

The preceding simulation showed that barometrically driven transport approaches a quasi-steady regime in which the fractional release is nearly the same for each successive cycle. This generally occurs by the time 10% of the contaminant has been expelled, suggesting that roughly 90% of the outflow can be predicted from a knowledge of the outflow parameter, $\dot{M}^*$, which is the reciprocal of the time constant for the exponential decay process of Equation (43).

Thus, the purpose of a quasi-steady analysis is to rapidly determine the fractional outflow rate $\dot{M}^*$ by performing a brief simulation which is begun with a linear contaminant profile. This choice of initial profile is based on the preceding simulation and others like them (Nilson *et al.*, 1991) which all appear to tend toward a relatively linear gradient as time progresses. The dotted line in Figure 11 depicts the linear distribution having the same contaminant inventory as the calculated profile corresponding to 160 years.

Quasi-steady calculations are executed with the same model as the earlier transient simulations except that: (1) the initial profile is now linear and, (2) the concentration at the floor of the medium is now held fixed at unity rather than prescribing that there be no contaminant flux through the floor. By fixing the concentration at the floor we prevent the gradual drift of the linear profile that would otherwise occur during depletion. Throughout the calculational period of 20 barometric cycles there is only a slight shift in the near-surface region of the linear concentration profile, reaffirming the connection between linear profiles and quasi-steady behavior. Much longer runs confirm the same behavior.

Figure 13 indicates that the effluent flux, $\dot{M}^*$, becomes quasi-steady within just a few days. Moreover, the predicted value of $\dot{M}^* \approx 0.003$ in Figure 13 is quite consistent with the corresponding value of $\dot{M}^* \approx 0.002$ near the end of the full simulation in Figure 12. The difference is attributed to the fact that linearity was

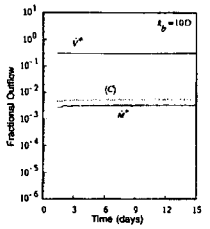

Figure 13. Normalized outflows for quasisteady analysis with typical YM parameters.

never fully established in the complete simulation. In this context it is noted that the $\dot{M}^*$ associated with a linear profile is insensitive to the choice of unit concentration at the floor of the medium, since the outflow, $\dot{M}^*$, is normalized by the total amount of contaminant present and the transport equations are linear in concentration. However, the mean concentration in the medium is reflected in the average concentration of the effluent $\langle X^* \rangle$ which differs by more than an order of magnitude between Figures 12 and 13 because the ratio of mean concentrations is $0.5/0.03 \sim 170$.

The advantage of quasi-steady analyses is that, parameter studies can be performed with a thousand-fold savings of computer time since the required calculations span several days rather than 15–150 years. This approach is particularly beneficial in cases with weak transport and large retardation factors which would otherwise require 10–100 times more computation than the 50 h run which generated Figure 12. The same savings cannot be realized by simply increasing the magnitude of the calculational time step, because it is constrained by the time scale of barometric cycles and by the Courant limitation imposed by virtually all nondiffusive advection algorithms. The only shortcoming of the quasi-steady simulations is that they do not explicitly reveal the time required for the profile to spread across the medium. However, this can be estimated after the fact since the quasi-steady calculations do indicate the strength of the transport and this, together with a knowledge of the capacitance, can be used to estimate the time required to reach quasi-steady state.

B.3. SINGLE-HORIZON MODELS

Having seen that the BP process evolves toward quasi-steady transport through a linear gradient, we will now briefly explore the use of analytical and numerical models

which seek to evaluate the rate of quasi-steady transport by solving the time dependent transport equations in a single, typical horizontal plane. The key supposition is that the vertical gradients appearing in the differential equations can be replaced by their time-mean values. This reduces the dimensionality of the problem from two to one. The associated reduction in computational effort is particularly beneficial in addressing the more complex multiphase flow processes that control barometric respiration of water vapor. The single-horizon model also helps to illuminate physical mechanisms and parametric dependencies.

To illustrate the nature and validity of a single-horizon model, we will consider a simplified version of the BP process in which the fracture walls are porous ($\phi_m \neq 0$) but impermeable ($k_m = 0$) so that horizontal contaminant transport occurs purely by molecular diffusion; there is no bulk flow in the horizontal direction. Conversely, the vertical transport in the fracture is presumed to be advection dominated, as expected in most applications. Under these simplifications, the transport is governed by the following pair of equations which respectively apply to the fracture and the matrix. Here, we introduce a modified diffusivity $D^* = D_0\beta/\phi_m$ to simplify subsequent equations:

$$\frac{\partial X}{\partial t} + u_{By}\frac{\partial X}{\partial y} = \phi_m D^* \frac{2}{w}\frac{\partial X}{\partial x}, \tag{45}$$

$$\phi_m \frac{\partial X}{\partial t} = \phi_m D^* \frac{\partial^2 X}{\partial x^2}. \tag{46}$$

These can be solved analytically if it is further assumed that the vertical velocity in the fracture is harmonic, i.e. $u_{By} = q_0 \Re\{\exp(i\omega t)\}$, and that the vertical concentration gradient is uniform. Both of these suppositions are consistent with the behavior observed in the earlier numerical simulations. Under these simplifications, Equation (45) describing species conservation within the fracture may now be viewed as a boundary condition on the single-horizon problem for the time-dependent variation of species concentration across the matrix material. To complete the single-horizon problem statement, it is also required that there be no fluxes across the center plane of the matrix slab since this is a plane of symmetry.

The exact solution to this prototype problem is the real part of the following complex function (Kurzweg, 1985; Nilson *et al.*, 1991):

$$X = \gamma\{y + bg(x)e^{i\omega t}\}, \tag{47}$$

in which $\gamma = \mathrm{d}X/\mathrm{d}y$ is the vertical concentration gradient, b is the half fracture spacing, and g is a complex function of the normalized depth into the wall $x^* = x/b$:

$$g = \frac{iq_0}{b\omega}\left(\frac{W\sqrt{i}}{W\sqrt{i} + \alpha \tanh W\sqrt{i}}\right)\frac{\cosh W\sqrt{i}(1 - x^*)}{\cosh W\sqrt{i}}. \tag{48}$$

Two dimensionless parameters appearing here are the Womersley number, $W = b\sqrt{\omega/D^*}$, and the ratio of pore volume to fracture volume, $\alpha = B\phi_m/w$. From

Equation (47), it is seen that the time mean concentration varies linearly with height, y, but is independent of depth into the wall, x. Further, the variation of concentration is sinusoidal at all locations with the amplitude and phase modulated by the depth into the wall, as embodied through the complex function $g(x^*)$.

The volume of fluid, $\Delta V = wq_0T/4\pi$, and corresponding mass of contaminant, ΔM, which pass through any horizontal plane during a single cycle of period T can be evaluated by time integration. As before, the ratio of these two integrals is used to define an effective mean concentration $\langle X \rangle$ which characterizes the net throughout of contaminant:

$$\langle X \rangle = \frac{\Delta M}{\Delta V} = \gamma \Delta L \Psi(W_\alpha, \alpha). \tag{49}$$

This mean concentration is of primary importance because it is linearly related to the vertical mass transport M^* in accordance with Equation (44). It depends upon the vertical gradient, $\gamma = \mathrm{d}X/\mathrm{d}y$, the amplitude of the vertical motion, $\Delta L = \Delta V/w = q_0T/4\pi$, and a dimensionless function $\Psi(W_\alpha, \alpha)$ of a modified Womersley number, $W_\alpha = W/\alpha$, and the volume ratio $\alpha = B\phi_m/w$ as indicated in the following equation:

$$\Psi(W_\alpha, \alpha) = -\frac{\pi}{4}\Re\mathrm{e}\left[\frac{W_\alpha\sqrt{i}}{W_\alpha\sqrt{i} + \tanh(\alpha W_\alpha\sqrt{i})}\right]. \tag{50}$$

As seen in Figure 14, there is a maximum rate of transport which depends somewhat on α but usually occurs for W_α near unity. For $W_\alpha \gg 1$, the period T is too short to allow a significant diffusive interaction between the fracture and the wall. Conversely, for $W_\alpha \ll 1$, the period is so long that the fracture and the wall are always nearly equilibrated in concentration; this also leads to a minimal net transport over a full cycle of motion. Thus, the transport is greatest when the period T is comparable to the

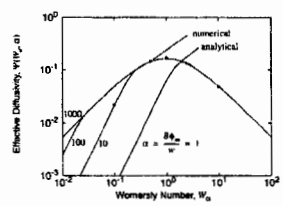

Figure 14. Comparison of the numerically computed single-horizon approximation (symbols) to the analytical solution given by Equation (50) for quasi-steady contaminant transport through a uniform gradient in a semi-infinite medium.

time required for molecular diffusion to access a pore volume which is comparable to the fracture volume.

Also included in Figure 14 are a series of symbols representing the results of numerical simulations performed by the computer code used in the main body of this paper to calculate water vapor transport. Since these calculations are in excellent agreement with the analytical solutions indicated by solid lines, we are confident that the numerical approach has been properly implemented, for this test problem at least.

A fundamental assumption of any such single-horizon modeling, analytical or numerical, is that the vertical concentration gradient, $\gamma = dX/dy$, can be taken as a constant. One might, however, expect that the flow along the fracture would perturb the gradient in an oscillatory fashion. Furthermore, it is implicitly presumed that the domain is of infinite extent in the direction of the concentration gradient. In the present application this implies infinite depth, so there is no opportunity to apply boundary conditions at the floor and the surface of the medium. This precludes the specification that there be no contaminant in the fresh air which flows into the fracture at the earth's surface. Instead, the concentration at every elevation, including the surface, oscillates sinusoidally about a mean value which increases linearly with depth. Although these simplifications of the model would appear to be well justified if the amplitude, ΔL, of the vertical motion were small compared to the depth, L, of the medium, they become questionable in the present application where $\Delta L/L$ sometimes exceeds unity, as apparent in Figure 8 where ΔL has a maximum value of about 1800 m for a layer having a depth of 600 m.

The validity of the single-horizon model was evaluated by comparing the above analytical solutions with two-dimensional numerical solutions which were posed on a domain of finite depth. In conformance with the analytical solutions, the vertical velocity was prescribed as sinusoidal in time and of equal amplitude at all elevations. However, in contrast to the analytical solutions, the numerical solutions satisfied more realistic boundary conditions with $X = 0$ for downflows from the upper surface and $X = 1$ for upflows from the bottom of the medium. Thus, the boundary condition at the earth's surface is identical to that used in the YM simulations where the atmosphere is idealized as an infinite reservoir of fresh air. For symmetry, the lower boundary is now idealized as an infinite reservoir of fully contaminated gas. Our goal is to determine whether the single-horizon model remains valid in cases where the vertical gradient is substantially perturbed from linearity and the gas displacements are as large as the vertical extent of the medium.

A series of numerical solutions were calculated for different values of the parameter $\Delta L/L$ with the other parameters held fixed at $W_a = 1.0$, $\alpha = 1.0$ and $\Delta X = 1.0$. Using these choices and the fact that $\gamma = \Delta X/L$, Equation (49) can be rewritten as $\langle X \rangle = \Psi(1, 1)\Delta L/L$. This analytical expression is plotted in Figure 15 along with the numerical results obtained in five different simulations. In each, the value of $\langle X \rangle$ was determined by time integration of the quantities defined in Equations (41) and (44), followed by substitution into Equation (44). It is seen that the numerical

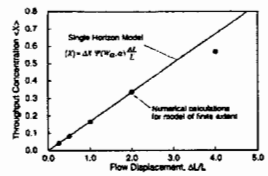

Figure 15. Comparison of single-horizon model with numerical calculations that take account of finite height and nonuniform gradients.

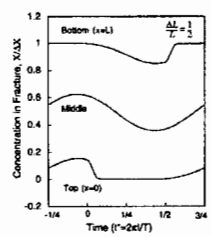

Figure 16. Concentration histories at three elevations for $\Delta L/L = 1/2$.

results are extremely close to the analytical solutions for $\Delta L/L \leqslant 2$. Even for displacements twice that large, the error in the single-horizon model is still less than 20% which is small compared to a number of other uncertainties involved in defining the problem of interest and the associated geologic parameters.

To better understand the success of the single-horizon model it is useful to further explore the details of the numerical solutions. Figures 16 and 17 show the numerical results for $\Delta L/L = 1/2$. The first of these indicates that the time variation at midheight follows a smooth sinusoidal path, in keeping with the analytical solution for an infinite domain. However, as expected, the time histories of concentration at the ends of the domain are far from sinusoidal, owing to the application of boundary conditions. In spite of this, the net flux is the same through all three elevations and it is nearly identical to the analytical prediction of Equation (49). Part of the explanation for this agreement is apparent in Figure 17 which shows that the slope of

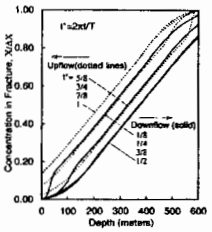

Figure 17. Concentration profiles at various times during typical cycle with $\Delta L/L = 1/2$.

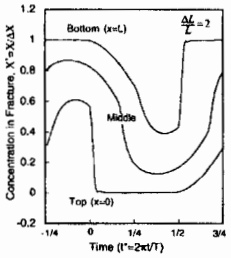

Figure 18. Concentration histories at three elevations for $\Delta L/L = 2$.

the concentration profile remains nearly constant despite significant displacements to the right and the left. If this slope were always to remain uniform and constant, we would be fully justified in replacing the vertical derivatives in the transport equations with their time mean values, as assumed in the single-horizon model. Thus, the results for moderate displacements are, in all respects, quite consistent with the analytical solutions, as expected.

However, what is somewhat surprising is that the single-horizon model closely predicts the numerical results shown in Figures 18 and 19 for $\Delta L/L = 2$. Here, there

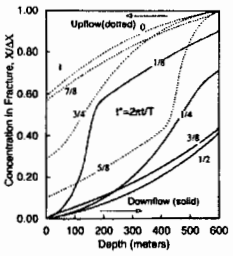

Figure 19. Concentration profiles at various times during typical cycle with $\Delta L/L = 2$.

are very significant departures from the mean gradient of $\gamma = \Delta X/L = 1$ which is presumed applicable in the analytical model. In spite of this, the single-horizon model provides an excellent prediction. Since the displacements of interest rarely exceed twice the layer depth, we have gained confidence in the use of this approach in modeling the more complex problem of moisture transport by BP, as discussed in the main body of this paper.

References

Bixler, N. E.: 1985. NORIA – A finite element computer program for analyzing water, vapor, air, and energy transport in porous media. Sandia National Laboratories Report. SAND84-2057, p. 115.

Church, H. W., Freeman, D. L., Boro, K. and Egami, R. T.: 1985. Meteorological tower data Yucca Ridge (YR) site. Sandia National Laboratories Report, SAND85-1053.

Church, H. W., Freeman, D. L., Boro, K. and Egami, R. T.: 1986. Meteorological tower data for the Yucca Alluvial (YA) site. Sandia National Laboratories Report, SAND86-2533.

Edlefsen, N. E. and Anderson, B. C.: 1943. Thermodynamics of soil moisture. *Hilgardia* **15**(2), 31–298.

Hyman, J. M.: 1979. A method of lines approach to the numerical solution of conservation laws. In: R. Vichnevetsky and R. S. Stepleman (eds), *Advances in Computer Methods for Partial Differential Equations III*. IMACS publications.

Kurzweg, U. H.: 1985. Enhanced heat conduction in oscillating viscous flow within parallel plate channels. *J. Fluid Mech.* **156**, 291–300.

Martinez, M. J.: 1995. Formulation and numerical analysis of nonisothermal multiphase flow in porous media. Sandia National Laboratories Report. SAND94-0379, Albuquerque, NM, June, p. 28.

Nilson, R. H. and Lie, K. H.: 1990, Double-porosity modeling of oscillatory gas motion and contaminant transport in a fractured porous medium, *Int. J. Numer. Anal. Meth. Geomech.* **14**, 565–585.

Nilson, R. H., Peterson, E. W., Lie, K. H., Burkhard, N. R. and Hearst, J. R.: 1991, Atmospheric pumping: a mechanism causing vertical transport of contaminated gases through fractured permeable media, *J. Geophys. Res.* **96**(B13), 21933–21948.

Nilson, R. H., Lagus, P. L., Mckinnis, W. B., Hearst, J. R., Burkhard, N. R. and Smith, C. F.: 1992, Field measurements of tracer gas transport induced by barometric pumping, In: *Proc. 1992 High Level Radioactive Waste Management Conference*, Las Vegas, Nevada (April 1992).

Pruess, K.: 1987, TOUGH user's guide, Lawrence Berkeley Laboratory Report, LBL-20700 (NUREG/CR-4645), August, p. 78.

Tsang, Y. W. and Pruess, K.: 1989, Preliminary studies of gas phase flow effects and moisture migration at Yucca Mountain, Nevada, Lawrence Berkeley Laboratory Report, LBL-28819, p. 42.

Tsang, Y. W. and Pruess, K.: 1990, Further modeling studies of gas movement and moisture migration at Yucca Mountain, Nevada, Lawrence Berkeley Laboratory Report, LBL-29127, p. 52.

Shampine L. F. and Watts, H. A.: 1980, DEPAC – Design of a user oriented package of ODE solvers, SAND79-2374, Sandia National Laboratories, Albuquerque, NM.

Somerton, W. H., Keese, J. A. and Chu, S. L.: 1974, Thermal behavior of unconsolidated oil sands, *SPEJ*, **14**(5).

Van Genuchten, R.: 1978, Calculating the unsaturated hydraulic conductivity with a new closed-form analytical model, In: *Water Resources Bulletin*, Princeton University Press, Princeton University, Princeton, NJ.

Wilson, M. L., Gauthier, J. H., Barnard, R. W., Barr, G. E., Dockery, H. A., Dunn, E., Eaton, R. R., Guerin, D. C., Lu, N., Martinez, M. J., Nilson, R. H., Rautman, C. A., Robey, T. H., Ross, B., Ryder, E. E., Schenker, A. R., Shannon, S. A., Skinner, L. H., Halsey, W. G., Gansemer, J., Lewis, L. C., Lamont, A. D., Triay, I. R., Meijer, A. and Morris, D. E.: 1994, Total-system performance assessment for Yucca Mountain – SNL second iteration (TSPA-1993), SAND93-2675, Sandia National Laboratories, Albuquerque, NM.

Zhao, T. S. and Cheng, P.: 1996, Oscillatory heat-transfer in a pipe subjected to a laminar reciprocating flow, *J. Heat Transfer* **118**(3), 592–597.